Proline-rich Region of Non-Muscle Myosin Light Chain Kinase Modulates Kinase Activity and Endothelial Cytoskeletal Dynamics

Patrick Belvitch, Djanybek Adyshev, Venkateswaran R Elangovan, Mary E Brown, Caitlin Naureckas, Alicia N Rizzo, Jessica H Siegler, Joe GN Garcia*, Steven M Dudek

Division of Pulmonary, Critical Care, Sleep, and Allergy

University of Illinois Hospital and Health Science System, Chicago, Illinois

*University of Arizona Health Sciences Center, Tucson, Arizona

***Corresponding Author**:

Steven M. Dudek, MD
Associate Professor of Medicine
Division of Pulmonary, Critical Care, Sleep and Allergy
University of Illinois Hospital and Health Sciences System
COMRB 3143, MC 719
909 S. Wolcott Ave.
Chicago IL 60612
Phone: 312-355-5887
Fax: 312-996-4665
Email: sdudek@uic.edu

ABSTRACT

Disruption of the pulmonary endothelial barrier and subsequent vascular leak is a hallmark of acute lung injury. Dynamic rearrangements in the endothelial cell (EC) peripheral membrane and underlying cytoskeleton are critical determinants of barrier function. The cytoskeletal effector protein non-muscle myosin light chain kinase (nmMLCK) and the actin-binding regulatory protein cortactin are important regulators of the endothelial barrier. In the present study we functionally characterize a proline-rich region of nmMLCK previously identified as the possible site of interaction between nmMLCK and cortactin. A mutant nmMLCK construct deficient in proline residues at the putative sites of cortactin binding (amino acids 973, 976, 1019, 1022) was generated. Co-immunoprecipitation studies in human lung EC transfected with wild-type or mutant nmMLCK demonstrated similar levels of cortactin interaction at baseline and after stimulation with the barrier-enhancing agonist, sphingosine 1-phosphate (S1P). In contrast, binding studies utilizing recombinant nmMLCK fragments containing the wild-type or proline-deficient sequence demonstrated a two fold increase in cortactin binding ($p<0.01$) to the mutant construct. Immunofluorescent microscopy revealed increased stress fiber density in ECs expressing GFP-labeled mutant nmMLCK at baseline ($p=0.02$) and after thrombin ($p=0.01$) or S1P ($p=0.02$) when compared to wild-type. Mutant nmMLCK demonstrated an increase in kinase activity in response to thrombin ($p<0.01$). Kymographic analysis demonstrated increased EC membrane retraction distance and velocity ($p<0.01$) in response to the barrier disrupting agent thrombin in cells expressing the mutant vs. wild-type nmMLCK construct. These results provide evidence that critical prolines within nmMLCK (amino acids 973, 976, 1019, 1022) regulate cytoskeletal and membrane events associated with pulmonary endothelial barrier function.

KEYWORDS: ARDS, Endothelium, Barrier Function, Cytoskeleton, non-muscle Myosin Light Chain Kinase, Cortactin, stress fibers, membrane dynamics

INTRODUCTION

The acute respiratory distress syndrome (ARDS) is a highly morbid clinical entity marked pathophysiologically by the flooding of the alveolar space with protein rich fluid which leads to severe impairment of gas exchange and hypoxia (Rubenfeld and Herridge, 2007; Ware and Matthay, 2000). Under normal conditions, the pulmonary endothelium forms a thin semipermeable barrier between the vascular space and the interstitial and alveolar spaces allowing for effective gas exchange while preventing the excess leakage of fluid and protein (Dudek and Garcia, 2001). However, this barrier becomes severely compromised during ARDS.

Pulmonary endothelial cell (EC) mechanics play a central role in the regulation of this barrier function as the formation of intercellular gaps and paracellular movement of fluid and solute are the primary mechanism producing vascular leak in pathologic conditions (Baldwin and Thurston, 2001; Garcia et al., 1995). The combination of EC shape and the formation of tight connections to neighboring cells through junctional proteins determine the degree of intercellular gap formation or closure and are affected by rearrangements of the EC cytoskeleton (Baldwin and Thurston, 2001; Birukova et al., 2009; Dudek and Garcia, 2001). Transcellular contractile forces generated by thick actin filaments termed stress fibers disrupt the EC barrier, while peripherally directed cell-cell and cell-matrix tethering forces seal paracellular gaps and increase barrier function (Dudek and Garcia, 2001). In vitro, the edema generating compound thrombin stimulates the formation of transcellular stress fibers, cell contraction, and rounding to disrupt the EC barrier (Bogatcheva et al., 2002; Garcia et al., 1996). In contrast, physiologic levels of the endogenous phospholipid sphingosine-1-phosphate (S1P) induce actin rearrangement to the cell periphery and formation of a cortical ring which significantly increases barrier function (McVerry and Garcia, 2004; Schaphorst et al., 2003). In addition, S1P increases peripheral areas of dynamic actin rearrangement to produce membrane

projections, such as lamellipodia, that decrease intercellular gaps and strengthen the EC barrier (Lee et al., 2006).

The actin dynamics that determine barrier function are controlled by a number of cytoskeletal regulatory proteins including cortactin (CTTN) and non-muscle myosin light chain kinase (nmMLCK) (Dudek et al., 2004). Cytoskeletal force generation is mediated by the ATP-dependant ratcheting of actin and myosin bonds catalyzed in EC by nmMLCK, a Ca^{2+}/calmodulin-dependent enzyme (Dudek and Garcia, 2001; Shen et al., 2010). This 1914 amino acid protein is similar to smooth muscle MLCK but with a unique N-terminal region (amino acids 1-923) containing multiple regulatory tyrosine phosphorylation sites for both Src and c-Abl (Dudek et al., 2010) (Garcia et al., 1995; Verin et al., 1998). The C-terminal half of the enzyme contains the catalytic, calmodulin-binding, KRP-binding, and myosin-binding domains (Garcia et al., 1997).

Cortactin is a 546 amino acid protein that participates in multiple aspects of cytoskeletal rearrangement to regulate EC elastic properties and barrier function (Arce et al., 2008; Li et al., 2004). CTTN contains multiple functional domains that regulate actin structure, including a binding site for filamentous actin and an N-terminal acidic domain that stimulates the Arp2/3 complex to polymerize branched actin filaments (Cosen-Binker and Kapus, 2006; Li et al., 2004). CTTN also contains multiple regulatory phosphorylation sites with serine and tyrosine residues located within a proline rich α-helix domain (Zhao et al., 2009). The C-terminus of CTTN consists of a Src homology 3 domain (SH3) that provides a site of interaction for numerous other EC proteins (Cosen-Binker and Kapus, 2006; Zarrinpar et al., 2003). CTTN rapidly translocates to sites of dynamic peripheral actin rearrangement after stimuli that increase EC barrier function (Brown et al., 2010), and inhibition of its expression impairs barrier enhancement by S1P (Lee et al., 2006) (Dudek et al., 2004).

Previous work has demonstrated an association between nmMLCK and CTTN through the latter protein's SH3 domain (Dudek et al., 2002; Dudek et al., 2004), and inhibition of this

interaction attenuates S1P-induced barrier enhancement (Dudek et al., 2004). Recombinant protein studies revealed no alterations in the enzymatic activity of nmMLCK in response to CTTN binding, but this interaction decreased the ability of nmMLCK to bind F-actin (Dudek et al., 2002). The putative sites of this interaction within nmMLCK were characterized using blocking antibodies and interfering peptides to identify amino acids #972-979 and #1019-1025 as the likely moieties responsible for this binding (Dudek et al., 2002). These sites contain proline rich sequences which conform well to consensus SH3 domain recognition motifs for the CTTN domain (Sparks et al., 1996). The goal of the present study was to characterize the functional effects of critical prolines within the CTTN binding site of nmMLCK to provide additional insights into how these key cytoskeletal proteins regulate EC barrier function.

MATERIALS AND METHODS

Reagents and antibodies

Reagents and chemicals were obtained from Sigma (St. Louis, MO) unless otherwise specified. Cortactin monoclonal antibody-4F11 was purchased from Millipore (Billerica, MA). Anti-Flag monoclonal antibody M5 was purchased from Sigma (St. Louis, MO). Anti-VE-cadherin mouse monoclonal antibody was purchased from Santa Cruz (Santa Cruz, CA). Fluorescent dye labeled reagents and Prolong Gold with DPI were obtained from Molecular probes (Eugene, OR). Cell culture reagents were purchased from Lonza (Walkersville, MD).

DNA Construct generation

The wild-type nmMLCK construct was subcloned from the previously described mammalian expression vector pJM1 (Moitra et al., 2008) as Acc65I-EcoRI fragment with N-terminal 6xFlag-tag into pcDNA3.1(+) mammalian expression vector (Life Technologies, Carlsbad, CA). Site directed mutagenesis of this wild-type nmMLCK construct was performed to generate proline to alanine substitutions at amino acid sites 973, 976, 1019 and 1022 by using the QuikChange Multi Site-Directed Mutagenesis kit (Agilent Technologies, Inc., Santa Clara, CA) according to the manufacturer's protocol (Figure 1A). Both wild-type and proline deficient mutant nmMLCK constructs were also subcloned into mammalian EGFP tagged expression vector pEGFP-C1 (Life Technologies, Carlsbad, CA). Both wild-type and proline deficient truncated nmMLCK fragments of 206 amino acids from #934-1140 containing the putative sites of CTTN binding were generated from the full length constructs by PCR. Primer sequences for truncated human nmMLCK, 5'- CACCAAGACTGTGTCTGAGGAA-3' (sense), containing the sequence CACC at the 5' end of the primer for the directional cloning and 5'-

TTAGGTGGTCTTGAGGGTCTTTC-3' (antisense) were designed by using NCBI Primer-BLAST tool (http://www.ncbi.nlm.nih.gov/tools/primer-blast/primerinfo.html) and subcloned into pENTR™/D-TOPO entry vector by directional TOPO cloning following subcloning by LR recombination to the pDEST™17 bacterial expression vector with N-terminal 6xHIS-tag according to the manufacturer's protocol (Life Technologies, Carlsbad, CA) (Figure 3A). Rat CTTN in pDsRed-N1 constructs were generously provided previously by Drs. Mark McNiven (MayoClinic) and H. Clive Palfrey (University of Chicago) for use in live cell imaging studies (McNiven et al., 2000).

In Silico Protein Modeling

The online application Protein Homology/analogy Recognition Engine (PHYRE) was used to analyze the 206 amino acid sequence of the recombinant wild type and proline deficient constructs and generate a model of the predicted structure (Kelley and Sternberg, 2009).

Cell Culture

Human pulmonary artery EC (HPAECs) (Lonza, Basel, Switzerland) were cultured in Endothelial Basal Medium (EBM)-2 complete medium with 10% fetal bovine serum (FBS) in a humidified incubator with 5% CO_2 at 37 degrees C as we have described previously (Dudek et al., 2004; Garcia et al., 2001). Passages 5-9 were used for experimentation. On the day of experimentation media was changed to serum free media and cells were treated as outlined in specific experimental conditions.

Transfection

ECs were transfected with mutant and wild-type constructs per manufacturer protocol using the X-fect transfection reagent purchased from Clontech (Mountain View, CA).

Co-immunoprecipitation

ECs were grown to confluence in 60 mm dishes as described above. Cells were then treated with either 1μM S1P or PBS for 10 minutes. Cells were washed three times with ice-cold PBS and lysed with 0.6 ml per dish of Co-IP lysis buffer (20 mM Tris-HCL; 150 mM Nacl; 1% NP-40; 2 mM EDTA; 0.5 mM PMSF; 0.2 mM sodium orthovanadate; 0.5% Protease and 0.5% phosphatase inhibitor cocktail (Calbiochem)). Cells were scraped and allowed to incubate for 15 min on ice. Cell lysates were passed through a 26G needle 10 times and centrifuged for 10 min at 15K rpm at 4 °C. Anti-Flag or anti-cortactin antibody was added (1:120) and incubated for overnight while rotating at 4 °C. The following day, 50 μL of protein G beads (GE Life Sciences, Pittsburgh, PA) were washed three times with Co-IP wash buffer (20 mM Tris-HCL; 150 mM Nacl; 1% NP-40; 2 mM EDTA; 2 mM EGTA; 0.2 mM sodium orthovanadate; 20 mM NaF; 1 mM sodium phosphate). Lysates were then added to beads and rotated at 4 °C for 1.5 hours. Beads were washed three times with Co-IP wash buffer and once with 20 mM Tris, pH 7.5. Protein was eluted off the beads with 90 μL 2x Laemlli sample buffer containing 2-β-mercaptoethanol [1:20] and boiled for 5 min at 100 °C.

Recombinant Protein Binding Studies

His-tagged nmMLCK fragment were purified from E.coli using an immobilized cobalt chelate kit per manufacturer protocol (Pierce Biotechnology, Rockford, IL). These purified samples were then dialyzed in TBS using a 10K MW G2 Membrane Dialysis Cassette to remove excess imidazole. Protein concentrations were measured using a BCA protein assay kit. A previously generated GST-tagged full length cortactin construct (Huang et al., 1997) was subjected to in vitro phosphorylation in a reaction buffer containing 50 mM Tris-HCl, pH 7.4, 5 mM MgCl2, 75 U/ml pp60Src, and 150 μ ATP. The reaction was carried out at room temperature for 60 min. Phosphorylated cortactin was then dissolved in an equilibration/wash buffer containing 125mM Tris and 150 mM sodium chloride at a pH of 8 and immobilized on glutathione agarose. His-tagged nmMLCK fragments were then incubated with the cortactin containing beads for 1 hour at 4°C. Agarose beads were then washed with equilibration/wash buffer a total of 5 times. Laemlli sample buffer containing 2-β-mercaptoethanol [1:20] was added to the beads-protein complex and boiled for 5 min at 100 °C to elute protein and dissolve the agarose. These samples were then subjected to western blotting. All kits, beads and dialysis products above were purchased from Pierce Biotechnology, Rockford, IL.

nmMLCK Activity Assay

EC were transfected with WT or mutant nmMLCK and grown to confluence in 10 cm^2 wells as described above. Cells were then treated with thrombin (1U/ml) or PBS x 5 minutes and washed with cold PBS x 3. Next, cells were lysed with RIPA buffer containing 0.5% Protease and 0.5% phosphatase inhibitor cocktail (Calbiochem)), scraped and allowed to incubate for 15 min on ice. The lysate was passed through a 26G needle x 10 and centrifuged at 15K rpm x 10 min at 4 °C. Anti-Flag antibody was added (1:120) and incubated overnight

while rotating at 4 °C. The following day 30 µl protein G beads (GE Life Sciences, Pittsburgh, PA) were added to lysates and incubated for 1 hour while rotating at 4 °C. Next, beads were washed x 3 in a buffer containing 20 mM Tris-HCL; 150 mM Nacl; 1% NP-40; 2 mM EDTA; 2 mM EGTA; 0.2 mM sodium orthovanadate; 20 mM NaF; 1 mM sodium phosphate. Beads were then hydrated in TBS and stored at -80 °C for later use. The isolated nmMLCK constructs were incubated with recombinant human MLC II, (0.5 µg/reaction, Gen Way Biotech, San Diego CA) in reaction buffer (12.5mM MgCl2, 5mM β-glycerol phosphate, 4 mM MOPS, 1mM EGTA, 25mM Tris-HCl (pH 7.5), 0.2 mM DTT, 300 µM $CaCl_2$, 1 µM calmodulin, 400 µM ATP and 0.5% Protease and 0.5% phosphatase inhibitor cocktail (Calbiochem)). The phosphorylation reaction was carried out at 37 °C for 30 minutes and terminated by the addition of 4x Laemmli sample buffer (Boston Bioproducts, Boston, MA). Samples were vortexed and boiled for 5 minutes. To determine nmMLCK activity samples were processed for western blot and probed with anti-phospho-MLC II thr 18 / ser 19 antibody (Cell Signaling, Danvers, MA).

Western blotting

Protein from co-immunoprecipitation and nmMLCK activity experiments were separated on a 10% or gradient 4-15% SDS-polyacrylamide gel and transferred to PVDF membrane. Membrane was blocked with a 5% telostean gelatin solution containing 2%BSA in TBS with 0.2% tween. Blots were incubated with primary antibodies overnight at 4 °C and secondary horseradish peroxidase-conjugated antibodies for 1 hour. Protein bands were visualized using ECL substrate (Pierce Biotechnology, Rockford, IL).

Immunofluorescent Studies

EC transfected with GFP-tagged nmMLCK wild-type and mutant constructs were grown in a 12-well plate containing a gelatin-coated 18–mm glass coverslip in each well. Cells were then treated with 1μM S1P, 1 U/ml thrombin or PBS for 10 minutes. Following treatment, coverslips were removed and washed in sterile PBS then immediately transferred to wells containing 4% paraformaldehyde/PBS, pH 7.4. Cells were fixed for 20 min at room temperature and then treated with 50 mM NH4CL/PBS, pH 7.4 for three 5 minute washes to quench unreacted aldehyde groups. Cells were blocked and permeabilized using 0.25% fish skin gelatin/0.01% saponin/0.1% NaN3/PBS, pH 7.4 (blocking solution) for 30 minutes at room temperature. Actin was stained using 5 U/ml phalloidin-rhodamine in blocking solution. As indicated, cells were treated with, anti-VE-cadherin mouse monoclonal antibody (Santa Cruz) diluted 1:100. Cells were incubated for 30 minutes in the dark. Fixed EC were then washed for 5 min x 3 in blocking solution and mounted in 10 μL Prolong Gold with DAPI and allowed to dry overnight in the dark. Cells were imaged the following day with a Zeiss 710 LSM confocal microscope with an alpha Plan-Apochromat 63X/1.46 NA oil Korr M27 objective lens. Cells were illuminated with a 405nm diode UV laser, 488 nm Ar laser, 561 nm solid-state diode laser, and 633nm He/Ne laser lines scanning with a pixel dwell time of 0.788 μsec and a line average setting of 4. Cells were illuminated sequentially scan line-by-scan line and emission bandwidths were limited to 411-472 for blue emission, 495-543 nm for green emission, 573-621nm for red emission, and 641-758 nm for far red emission. Pinhole diameters were 1.59, 1.35, 1.18, and 1.00 airy units for all four laser lines, respectively. Twelve-bit grayscale 1024x1024 images were collected with a pixel size of 132 nm. Focal planes with the most uniform signal emission simultaneously across all four channels were chosen. Grayscale images were recombined into color images and all other post-acquisition image processing was performed with Fiji (http://fiji.sc/wiki/index.php/Fiji).

Stress Fiber Quantification

Stress fiber density was measured using *ImageJ* similar to a method described previously (Peacock et al., 2007). Briefly, TIFF images were converted to 8-bit grayscale and the threshold tool was used to set an OD limit that captured most F-actin bundles. One investigator (AR) was blinded to the experimental conditions and drew a ROI line perpendicular to the longitudinal axis through each cell center and at points of membrane tethering. The plot profile function was then used to generate average pixel intensity along the line of interest. The density was then calculated by measuring the area under the curve of pixel intensity above the threshold limit divided by the total area.

Live cell imaging

EC were plated onto gelatin coated 25 mm coverslips, loaded into a recording chamber (ALA Scientific Instruments, Wesbury, NY) and overlayed with a batch solution containing EBM/2%FBS. The recording chamber was placed on a heated stage to maintain a temperature of 37 °C. A Zeiss 710 laser scanning confocal microscope was used for all imaging. Images were acquired every 6 seconds and cells were observed under basal conditions, after treatment with 1 U/ml thrombin x 15 minutes and then for 20-30 minutes after administration of 1μM S1P. Images were analyzed using *ImageJ* and kymographic analysis was performed using the Multiple Kymograph pluggin to assess membrane dynamics as described previously (Doggett and Breslin, 2011; Ott and Lippincott-Schwartz, 2012; Yi et al., 2011).

Statistical Analysis

Data are represented as group means +/- SEM. Statistical significance was determined using one-way ANOVA or t-test as appropriate. Stress fiber density and membrane retractions were analyzed with the non-parametric Mann-Whitney test. In all cases statistical significance was defined as $p<0.05$.

RESULTS

Effect of nmMLCK Proline Residues on Cortactin Co-Immunoprecipitation

In order to better characterize the putative site of CTTN binding within nmMLCK, site directed mutagenesis was employed to generate a novel construct with key proline residues mutated to alanine. A total of four prolines were mutated to alanine, two at each potential CTTN SH3 binding site (Figure 1A). Wild-type and mutant flag-tagged constructs were then transfected into HPAECs, stimulated with vehicle control or S1P x 10 minutes, immunoprecipitated with anti-flag antibodies, and then CTTN levels in the isolated protein complexes were determined by western blotting. In reciprocal experiments, anti-CTTN antibodies were used for immunoprecipitation, and then the isolated protein complex was probed for associated flag-tagged nmMLCK constructs. Based upon previous studies (Dudek et al., 2002; Dudek et al., 2004), we hypothesized that elimination of these prolines would result in decreased CTTN binding. However, after adjusting for the level of immunoprecipitated protein, no significant differences in cortactin interaction were observed in cells expressing the mutant nmMLCK protein under basal conditions or after stimulation with S1P ($p=0.77$) (Figure 1B-D).

nmMLCK Proline Residues Modulate Direct Binding to Recombinant Cortactin

Because co-IP studies may involve multiple proteins within a complex and not represent direct interaction between specific proteins, we next generated recombinant HIS-tagged nmMLCK fragments. The recombinant protein consisted of a nmMLCK fragment from #934-1140 encompassing the putative sites of interaction with CTTN at amino acids #972-979 and #1019-1025. Wild-type and mutant constructs were identical with the exception of the mutation of four critical prolines to alanine (Figure 2A). In silico modeling of the 206 amino acid nmMLCK

fragment #934-1140 revealed significant structural differences between the wild-type and proline-deficient constructs (Figure 2B) (Kelley and Sternberg, 2009). The model shows a more compact protein structure, particularly near the N-terminus, in the mutant fragment as compared to the wild-type fragment. The analysis also predicted the loss of several beta strand formations in the mutant fragment (Figure 2B). We employed a GST-tagged full length CTTN (Huang et al., 1997) to determine its direct interactions with the nmMLCK fragments. Because phosphorylation of three tyrosine sites within CTTN alters its conformation to allow increased interaction of its SH3 domain with other proteins, including nmMLCK (Ammer and Weed, 2008; Dudek et al., 2002), GST-CTTN was phosphorylated in vitro with Src prior to being immobilized onto glutathione beads and then incubated with the nmMLCK fragments. After normalization for the amount of immobilized CTTN, Western blotting revealed significantly increased binding of the proline-deficient mutant nmMLCK compared to the wild-type fragment ($p<0.01$) (Figure 2C-D).

nmMLCK Proline Residues Modulate EC Actin Structure and Membrane Dynamics

To explore the functional consequences of the proline-deficient nmMLCK mutant on EC cytoskeletal structure and membrane dynamics, we generated GFP-tagged wild-type and mutant nmMLCK constructs. HPAEC were transfected with these constructs and then fixed and stained for F- actin with phalloidin. The distribution of GFP-nmMLCK was consistent with previously described patterns (Brown et al., 2010) demonstrating diffuse staining under basal conditions and localization to transcellular stress fibers after thrombin (1U/ml x 10 min) treatment (Figure 3A GFP cells). These studies were not designed to assess peripheral lamellipodia but nmMLCK was observed to move to a more peripheral location after S1P (1 μM x 10 min) stimulation similar to previous studies (Brown et al., 2010). Interestingly, EC

transfected with wild-type nmMLCK demonstrated an increase in peripheral GFP-nmMLCK distribution when compared to EC expressing the mutant construct during both basal conditions and after S1P treatment. There were no apparent differences in GFP-nmMLCK distribution between wild-type and mutant after thrombin treatment.

Stress fibers were then quantified in transfected EC by using *ImageJ* software to assess actin filament density as described in Methods. Under basal conditions and following thrombin as well as S1P treatmentEC expressing the mutant nmMLCK construct exhibited significantly higher stress fiber density when compared to wild-type ($p<0.05$). (Figure 3B). Additionally, differential effects on actin distribution were observed following S1P with increased peripheral cortical actin in EC transfected with wild-type nmMLCK, a phenotype associated with barrier enhancing stimuli (Dudek and Garcia, 2001; Garcia et al., 2001) (Figure 3A Gray Scale images) (see also Supplemental Video) .

Peripheral cytoskeletal structure and membrane dynamics are important determinants of EC shape and barrier function (Baldwin and Thurston, 2001; Dudek and Garcia, 2001). Exposure of EC to the barrier-disrupting agent thrombin (1U/ml) produces rapid changes in cell shape and leads to contractions of the peripheral membrane (Bogatcheva et al., 2002; Garcia et al., 1996). To quantify these changes in membrane dynamics, HPAECs transfected with GFP-tagged wild type and proline-deficient nmMLCK constructs were subjected to kymographic analysis as described in Methods. EC expressing mutant nmMLCK exhibited significantly increased membrane retraction distance and velocity after thrombin compared to EC transfected with the wild-type construct ($p<0.01$) (Figure 4). Such increases in membrane retraction speed and magnitude are suggestive of a more barrier disruptive phenotype after thrombin (Vandenbroucke et al., 2008). Live cell imaging further illustrates these effects of the proline-deficient nmMLCK. EC expressing mutant nmMLCK exhibit more stress fibers and

overall cell contraction than those expressing wild type nmMLCK, while the latter display more cortical actin and lamellipodia formation (Supplementary Video).

Effect of nmMLCK Proline Residues on Kinase Activity

To further explore the differential effects observed between wild-type and proline-deficient nmMLCK on stress fiber formation and membrane dynamics, we next conducted kinase activity assays as described in Methods. Briefly, EC were transfected with flag-tagged wild-type or mutant nmMLCK constructs and treated with thrombin (1U/ml) or PBS for 5 minutes. Cells were lysed and flag-nmMLCK isolated by immunoprecipitation. Recombinant MLC in an activity assay buffer containing ATP, calcium and calmodulin was then added to the isolated protein and incubated for 30 minutes. Non-muscle MLCK kinase activity was determined by the degree of MLC phosphorylation as measured by western blot. As expected both wild-type and mutant nmMLCK exhibited increased kinase activity after thrombin treatment ($p<0.01$) (Figure 5A). Interestingly, an increase in the relative activity of proline-deficient nmMLCK was observed after thrombin treatment when compared to wild-type ($p<0.01$). In addition, there was a trend toward increased basal kinase activity in the mutant nmMLCK, but this effect did not reach statistical significance ($p=0.08$).

Effect of Proline Residues on VE-cadherin Distribution

The observed effects of nmMLCK proline to alanine substitution on stress fiber formation, membrane retraction and kinase activity suggest possible regulation of EC monolayer function (Baldwin and Thurston, 2001; Dudek and Garcia, 2001; Vogel and Malik, 2012). It is well described that thrombin and other barrier disruptive compounds interrupt the continuity of

adherens junctions, which can be visualized by immunofluorescent microsopy (Adamson et al., 2002; Vogel and Malik, 2012). To begin to address the functional effects of this substitution on barrier function, VE-cadherin distribution in wild type and mutant nmMLCK transfected cells was investigated as an assay of junctional integrity. HPAEC were transfected with GFP-tagged wild-type and proline-deficient nmMLCK, stimulated with vehicle or thrombin, and then fixed and stained for VE-cadherin. A decrease in VE-cadherin staining intensity and peripheral continuity in response to thrombin was observed, but there were no obvious differences in these patterns between cells transfected with wild-type or proline-deficient constructs (Figure 6).

DISCUSSION

The role of cytoskeletal rearrangement in determination of endothelial barrier function has been studied extensively (Arce et al., 2008; Baldwin and Thurston, 2001; Dudek and Garcia, 2001; Garcia et al., 1995; Shen et al., 2010; Shen et al., 2009), but translation of this knowledge into clinically relevant interventions remains an elusive goal. Prior work has demonstrated important roles for the cytoskeletal proteins CTTN and nmMLCK in regulating EC barrier function (Bryce et al., 2005; Dudek et al., 2004; Garcia et al., 1995). Although these proteins interact directly (Dudek et al., 2002), have been implicated in multiple functional processes (Garcia et al., 1995; Shen et al., 2010) (Arce et al., 2008) (Ammer and Weed, 2008; Cosen-Binker and Kapus, 2006), are targets of similar tyrosine kinases (Dudek et al., 2010; Dudek et al., 2004; Zhao et al., 2009), and share several binding partners (Ammer and Weed, 2008; Kamm and Stull, 2001), how their interaction is regulated and affects EC cytoskeletal structure and function remains incompletely defined. Improved understanding of these aspects of CTTN-nmMLCK interaction will advance our mechanistic knowledge of EC barrier regulation.

Prior work has demonstrated that interaction between nmMLCK and CTTN occurs through the latter protein's SH3 domain and that this interaction has functional implications for EC permeability and nmMLCK-F-actin binding (Dudek et al., 2002; Dudek et al., 2004). Two putative sites for this interaction within nmMLCK were identified using blocking antibodies and interfering peptides: amino acids #972-979 and #1019-1025 (Dudek et al., 2002). These sites contain proline rich sequences which conform well to consensus SH3 domain recognition motifs for CTTN (Sparks et al., 1996). In the current study we present additional data supporting an important functional role for these sites. First, elimination of these prolines by site-directed mutation in nmMLCK fragments results in increased CTTN-nmMLCK interaction in purified protein studies (Figure 2). Interestingly, co-immunoprecipitation studies using full length wild-type and mutant nmMLCK do not demonstrate any difference in CTTN interaction (Figure 1).

These co-immunoprecipitation results are seemingly in conflict with previous work demonstrating decreased CTTN binding when these sites within nmMLCK are blocked with antibody or peptides (Dudek et al., 2002), as well as the results obtained with direct recombinant CTTN protein binding to the nmMLCK fragments (Figure 2). There are several potential explanations for this apparent discrepancy. First, the proline sites mutated in this study may not be the location of direct CTTN binding but instead alter the tertiary structure of full length nmMLCK at a distant interaction site to regulate binding. Little is known about the tertiary structure of the 1914 amino acid nmMLCK enzyme, but in silico modeling of a 206 amino acid fragment encompassing these prolines supports the hypothesis that these sites have important structural consequences (Figure 2B). Another explanation, and more consistent with previously mentioned blocking studies, the mutations may alter nmMLCK structure locally in a manner that increases rather than inhibits CTTN binding at the putative SH3 binding sites (amino acids #972-979 and #1019-1025). This is supported by purified nmMLCK fragment experiments (Figure 2). The lack of altered interaction between full length mutant nmMLCK and CTTN in the co-immunoprecipitation experiments may be due to the multiple binding partners common to the two proteins, actin for example, and subsequent complex formation rather than a reflection of direct interaction between nmMLCK and CTTN. Alternately, the proline to alanine substitutions may have differentially altered the tertiary structures of the full-length and fragment nmMLCK leading to the increased association with CTTN observed in the fragment studies.

The importance of these proline sites is further demonstrated by the effects on EC cytoskeletal structure and function observed after mutating them to alanines. Our results demonstrate an increase in stress fiber density at baseline and after thrombin or S1P treatment (Figure 3) and more robust membrane retractions in response to thrombin (Figure 4) in EC transfected with proline deficient mutant nmMLCK relative to wild type. Live cell imaging further demonstrates these observations (Supplementary Video). Altered nmMLCK-CTTN interaction is

one possible explanation for these findings. As an actin stabilizing protein (Cosen-Binker and Kapus, 2006; Li et al., 2004), CTTN may create a persistent association between nmMLCK and actin stress fibers to increase centripetal force generation across the cell. Key prolines within nmMLCK (amino acids 973, 976, 1019, 1022) may serve to moderate CTTN interaction in a manner that also regulates actin stress fiber contraction.

These prolines may also regulate other aspects of nmMLCK function. Proline-deficient nmMLCK exhibits increased kinase activity after thrombin treatment (Figure 5), which is consistent with the observed increases in stress fiber formation and membrane retraction that occur in EC expressing this construct (Figures 3-4). However, the mechanism by which these prolines affect kinase activity remains unclear. Although these proline residues are approximately 500 amino acids away from the catalytic site, the 3D structure of full length nmMLCK is unknown, so it is possible that deleting these 4 prolines alters the catalytic pocket in a manner that directly increases activity. Other possible mechanisms include altering nmMLCK structure to increase protein-protein interactions (e.g., actin or MLC binding) or phosphorylation events to facilitate kinase activity. Previous studies conducted in isolation with recombinant protein indicate the interaction with CTTN does not modulate the kinase activity of nmMLCK (Dudek et al., 2002). However, it is possible an altered CTTN-nmMLCK interaction may produce differential activation of nmMLCK within cells leading to the increased kinase activity observed in the present study. The mechanism by which these prolines regulate nmMLCK kinase activity will be the focus of future studies.

While much is known regarding the structure, regulation and binding partners of CTTN, it's precise functional role in regulation of cytoskeletal dynamics is unclear (Cosen-Binker and Kapus, 2006). For example, CTTN and MLCK are found colocalized within complexes necessary for membrane retraction following osmotic swelling (Barfod et al., 2011). While nmMLCK is generally seen as barrier disruptive in its ability to catalyze the actin-myosin

interaction and drive cell contraction (Dudek and Garcia, 2001; Garcia et al., 1996), its enzymatic activity is also required for actin rearrangement and generation of membrane protrusions or lamellipodia in response to barrier enhancing stimuli (Dudek et al., 2004). However, a comprehensive understanding of the regulatory roles of nmMLCK, CTTN, and their interaction on cell shape and barrier function remains unclear.

There are a number of important limitations of our current study. First, the co-Immunoprecipitation experiments using full length nmMLCK were carried out in EC expressing endogenous levels of CTTN and nmMLCK that may influence the observed effects of overexpressing proline-deficient and wild type nmMLCK. Second, the purified nmMLCK fragments and full length cortactin construct used for recombinant protein binding studies were synthesized via a bacterial expression system which may alter posttranslational modifications as compared to eukaryotic expression, most notably in protein phosphorylation (Sahdev et al., 2008). Third, while techniques were employed to quantify stress fibers and membrane dynamics objectively, significant biological variability in cell responses make the selection of regions of interest for analysis a somewhat subjective process that could influence results. Finally, the potential regulatory effects of the nmMLCK proline-rich region on EC barrier function have not been determined. Unfortunately, the transfection method employed in these studies results in a maximal transfection efficiency of <10% of the cells expressing the full length nmMLCK constructs. This low expression percentage precludes accurate evaluation of possible permeability effects across an intact monolayer using cell impedance or labeled tracer transwell assays. Future work may employ viral vectors to generate high infection percentages and assess EC monolayer barrier function.

In conclusion, this study advances our structural understanding about the interaction between CTTN and nmMLCK, two important cytoskeletal proteins that participate in dynamic EC rearrangements regulating pulmonary vascular barrier function and vascular leak. These

data demonstrate that mutation of critical prolines in nmMLCK increases CTTN binding in purified nmMLCK fragments and increases stress fiber density at baseline as well as after thrombin and S1P in cells expressing mutant full length nmMLCK. Additionally, proline to alanine substitution increased nmMCK kinase activity and resulted in increased cell membrane retraction distance and velocities in response to thrombin. Thus, this region of nmMLCK is essential for modulating EC cytoskeletal responses to barrier regulatory stimuli and is worthy of further exploration.

REFERENCES

Adamson, R. H., et al., 2002. Rho and rho kinase modulation of barrier properties: cultured endothelial cells and intact microvessels of rats and mice. J Physiol. 539**,** 295-308.

Ammer, A. G., Weed, S. A., 2008. Cortactin branches out: roles in regulating protrusive actin dynamics. Cell Motil Cytoskeleton. 65**,** 687-707.

Arce, F. T., et al., 2008. Regulation of the micromechanical properties of pulmonary endothelium by S1P and thrombin: role of cortactin. Biophys J. 95**,** 886-94.

Baldwin, A. L., Thurston, G., 2001. Mechanics of endothelial cell architecture and vascular permeability. Crit Rev Biomed Eng. 29**,** 247-78.

Barfod, E. T., et al., 2011. Myosin light chain kinase and Src control membrane dynamics in volume recovery from cell swelling. Mol Biol Cell. 22**,** 634-50.

Birukova, A. A., et al., 2009. Endothelial permeability is controlled by spatially defined cytoskeletal mechanics: atomic force microscopy force mapping of pulmonary endothelial monolayer. Nanomedicine. 5**,** 30-41.

Bogatcheva, N. V., et al., 2002. Molecular mechanisms of thrombin-induced endothelial cell permeability. Biochemistry (Mosc). 67**,** 75-84.

Brown, M., et al., 2010. Quantitative distribution and colocalization of non-muscle myosin light chain kinase isoforms and cortactin in human lung endothelium. Microvasc Res. 80**,** 75-88.

Bryce, N. S., et al., 2005. Cortactin promotes cell motility by enhancing lamellipodial persistence. Curr Biol. 15**,** 1276-85.

Cosen-Binker, L. I., Kapus, A., 2006. Cortactin: the gray eminence of the cytoskeleton. Physiology (Bethesda). 21**,** 352-61.

Doggett, T. M., Breslin, J. W., 2011. Study of the actin cytoskeleton in live endothelial cells expressing GFP-actin. J Vis Exp.

Dudek, S. M., et al., 2002. Novel interaction of cortactin with endothelial cell myosin light chain kinase. Biochem Biophys Res Commun. 298**,** 511-9.

Dudek, S. M., et al., 2010. Abl tyrosine kinase phosphorylates nonmuscle Myosin light chain kinase to regulate endothelial barrier function. Mol Biol Cell. 21**,** 4042-56.

Dudek, S. M., Garcia, J. G., 2001. Cytoskeletal regulation of pulmonary vascular permeability. J Appl Physiol. 91**,** 1487-500.

Dudek, S. M., et al., 2004. Pulmonary endothelial cell barrier enhancement by sphingosine 1-phosphate: roles for cortactin and myosin light chain kinase. J Biol Chem. 279**,** 24692-700.

Garcia, J. G., et al., 1995. Regulation of endothelial cell gap formation and barrier dysfunction: role of myosin light chain phosphorylation. J Cell Physiol. 163**,** 510-22.

Garcia, J. G., et al., 1997. Myosin light chain kinase in endothelium: molecular cloning and regulation. Am J Respir Cell Mol Biol. 16**,** 489-94.

Garcia, J. G., et al., 2001. Sphingosine 1-phosphate promotes endothelial cell barrier integrity by Edg-dependent cytoskeletal rearrangement. J Clin Invest. 108**,** 689-701.

Garcia, J. G., et al., 1996. Regulation of thrombin-mediated endothelial cell contraction and permeability. Semin Thromb Hemost. 22**,** 309-15.

Huang, C., et al., 1997. Down-regulation of the filamentous actin cross-linking activity of cortactin by Src-mediated tyrosine phosphorylation. J Biol Chem. 272**,** 13911-5.

Kamm, K. E., Stull, J. T., 2001. Dedicated myosin light chain kinases with diverse cellular functions. J Biol Chem. 276**,** 4527-30.

Kelley, L. A., Sternberg, M. J., 2009. Protein structure prediction on the Web: a case study using the Phyre server. Nat Protoc. 4**,** 363-71.

Lee, J. F., et al., 2006. Sphingosine-1-phosphate signaling regulates lamellipodia localization of cortactin complexes in endothelial cells. Histochem Cell Biol. 126**,** 297-304.

Li, Y., et al., 2004. Interaction of cortactin and Arp2/3 complex is required for sphingosine-1-phosphate-induced endothelial cell remodeling. Exp Cell Res. 298**,** 107-21.

McNiven, M. A., et al., 2000. Regulated interactions between dynamin and the actin-binding protein cortactin modulate cell shape. J Cell Biol. 151**,** 187-98.

McVerry, B. J., Garcia, J. G., 2004. Endothelial cell barrier regulation by sphingosine 1-phosphate. J Cell Biochem. 92**,** 1075-85.

Moitra, J., et al., 2008. A transgenic mouse with vascular endothelial over-expression of the non-muscle myosin light chain kinase-2 isoform is susceptible to inflammatory lung injury: role of sexual dimorphism and age. Transl Res. 151**,** 141-53.

Ott, C., Lippincott-Schwartz, J., 2012. Visualization of live primary cilia dynamics using fluorescence microscopy. Curr Protoc Cell Biol. Chapter 4**,** Unit 4 26.

Peacock, J. G., et al., 2007. The Abl-related gene tyrosine kinase acts through p190RhoGAP to inhibit actomyosin contractility and regulate focal adhesion dynamics upon adhesion to fibronectin. Mol Biol Cell. 18**,** 3860-72.

Rubenfeld, G. D., Herridge, M. S., 2007. Epidemiology and outcomes of acute lung injury. Chest. 131**,** 554-62.

Sahdev, S., et al., 2008. Production of active eukaryotic proteins through bacterial expression systems: a review of the existing biotechnology strategies. Mol Cell Biochem. 307**,** 249-64.

Schaphorst, K. L., et al., 2003. Role of sphingosine-1 phosphate in the enhancement of endothelial barrier integrity by platelet-released products. Am J Physiol Lung Cell Mol Physiol. 285**,** L258-67.

Shen, Q., et al., 2010. Myosin light chain kinase in microvascular endothelial barrier function. Cardiovasc Res. 87**,** 272-80.

Shen, Q., et al., 2009. Endothelial contractile cytoskeleton and microvascular permeability. Cell Health Cytoskelet. 2009**,** 43-50.

Sparks, A. B., et al., 1996. Distinct ligand preferences of Src homology 3 domains from Src, Yes, Abl, Cortactin, p53bp2, PLCgamma, Crk, and Grb2. Proc Natl Acad Sci U S A. 93**,** 1540-4.

Vandenbroucke, E., et al., 2008. Regulation of endothelial junctional permeability. Ann N Y Acad Sci. 1123**,** 134-45.

Verin, A. D., et al., 1998. Biochemical regulation of the nonmuscle myosin light chain kinase isoform in bovine endothelium. Am J Respir Cell Mol Biol. 19**,** 767-76.

Vogel, S. M., Malik, A. B., 2012. Cytoskeletal dynamics and lung fluid balance. Compr Physiol. 2**,** 449-78.

Ware, L. B., Matthay, M. A., 2000. The acute respiratory distress syndrome. N Engl J Med. 342**,** 1334-49.

Yi, K., et al., 2011. Dynamic maintenance of asymmetric meiotic spindle position through Arp2/3-complex-driven cytoplasmic streaming in mouse oocytes. Nat Cell Biol. 13**,** 1252-8.

Zarrinpar, A., et al., 2003. The structure and function of proline recognition domains. Sci STKE. 2003**,** RE8.

Zhao, J., et al., 2009. Phosphotyrosine protein dynamics in cell membrane rafts of sphingosine-1-phosphate-stimulated human endothelium: role in barrier enhancement. Cell Signal. 21**,** 1945-60.

FIGURE LEGENDS

Figure 1. Proline to alanine mutations in full length nmMLCK do not alter co-immunoprecipitation of cortactin. (A)The two putative proline-rich CTTN binding sites within MLCK are shown (gray rectangles) within the protein schematic. Site directed mutagenesis resulted in the substitution of specific proline residues (underlined in italics) for alanine (gray). The mutant construct consists of four prolines changed to alanine, two at each site. (B) Representative western blot of HPAEC lysates after nmMLCK immunoprecipitation using flag antibody and blotted for flag-tagged MLCK and endogenous CTTN. (C) Western blot of the reciprocal experiment after cortactin immunoprecipitation. (D and E) Densitometric quantification of CTTN relative to immunoprecipitated nmMLCK (D), or nmMLCK relative to immunoprecipitated CTTN (E), is shown. Interaction between wild type (WT) nmMLCK and CTTN in the unstimulated condition (Con) is arbitrarily set at 1.0. Mutant nmMLCK demonstrates no significant change in co-immunoprecipitation with CTTN at baseline or after S1P x 10 min. N = 3-8 independent experiments per condition. Standard error bars are shown.

Figure 2. Mutant nmMLCK fragments exhibit increased binding to cortactin. (A) Structure of nmMLCK recombinant protein fragment and amino acid substitutions in mutant construct. The two putative proline-rich CTTN binding sites are shown (rectangles) within the fragment schematic. The mutated fragment was derived from the full length nmMLCK construct with specific proline residues (underlined in italics) changed to alanine (gray). (B) In silico modeling of the structure of a recombinant 206 amino acid nmMLCK fragment with the wild-type proline residues or mutant alanine residues at position #973, 976, 1019 and 1022. The fragments are composed of amino acid #934-1140 in the full length proteins. The color scheme depicts the N to C orientation of the protein on the color spectrum with red representing the amino terminus and violet the carboxy terminus. Regions predicted to form beta strands are depicted by the broad arrows. The models demonstrate a more compact structure, particularly at the N terminus, and loss of several beta strands in the mutant fragment as compared to the wild-type fragment. (C) Representative western blot of isolated protein interaction experiment. Purified GST-tagged CTTN was phosphorylated in vitro by Src kinase and immobilized on glutathione beads. After incubation with wild type or mutant HIS-tagged nmMLCK, beads were washed several times, boiled and proteins separated by electrophoresis. (D) Densitometric quantification of bound nmMLCK relative to the amount of CTTN is shown. Interaction between wild type (WT) nmMLCK and CTTN is arbitrarily set at 1.0. Significantly more cortactin was bound to the nmMLCK fragments containing the proline to alanine substitutions than to the wild type nmMLCK fragments (*$p<0.01$). N = 3 independent experiments per condition. Standard error bars are shown. MLC, myosin light chain binding site; CaM, calmodulin binding domain; KRP, kinase-related protein binding site; N, N-terminus; C, C-terminus.

Figure 3. Overexpression of mutant nmMLCK results in increased stress fiber density. (A) Representative images of EC transfected with GFP- tagged wild-type or mutant nmMLCK under basal conditions and after treatment with thrombin (1U/ml x 10 min) or S1P (1μM x 10 min). Images demonstrate nmMLCK localization to stress fibers after thrombin. Phalloidin-labeled actin fibers are shown in gray. Three transcellular line profiles per cell (center and each end) were drawn (yellow) for stress fiber quantification. Representative transcellular line profiles of optical density along the line of interest are shown to the right of each cell demonstrating increased area above threshold level (red dashed line) and altered distribution of stress fibers in the mutant construct. (B) Quantification of multiple cells demonstrating significantly increased stress fiber density at baseline, after thrombin and S1P treatment in cells expressing the mutant

nmMLCK construct when compared to cells expressing wild-type nmMLCK (*p<0.05). N = 5-8 cells analyzed per condition. Standard error bars are shown.

Figure 4. Mutations in nmMLCK increase membrane retraction distance and velocity in response to thrombin. (A and B) Kymographs generated from live cell imaging of HPAEC transfected with GFP-tagged wild type or mutant nmMLCK and treated with thrombin (1U/ml) for 10 minutes. Briefly, a region of interest (ROI) line (yellow) is drawn perpendicular to the membrane edge and parallel to its direction of motion. This is used to track the position of the membrane edge (x-axis) over time (y-axis) which is graphically represented by the grayscale image (kymograph) to the right of each cell. The slope of the kymograph (red line) at various points can be used to calculate the velocity of membrane retractions or protrusions. Cells transfected with mutant nmMLCK demonstrated significantly greater membrane retraction distances (C) and velocities (D) in response to thrombin when compared to wild type cells (*p<0.01). N = 3 cells analyzed to generate 5-8 kymographs per cell in each condition. Standard error bars are shown.

Figure 5. Mutations in nmMLCK increase kinase activity. (A) Quantification of relative nmMLCK activity in wild-type (WT) and mutant (Mut) constructs at baseline and after treatment with thrombin. EC were transfected with wild-type or mutant flag-tagged nmMLCK constructs and treated with thrombin (1U/ml x 5 min) or PBS (control). nmMLCK was then immunoprecipitated, recombinant MLC added, and MLC phosphorylation determined by Western blot as described in Methods. Relative activity was determined by normalizing the amount of MLC phosphorylation to precipitated nmMLCK, with the WT control arbitrarily set to 1.0. Both WT and mutant nmMLCK exhibited a significant increase in kinase activity after thrombin treatment as compared to control (*p<0.05) and mutant nmMLCK demonstrated significantly increased kinase activity after thrombin when compared to WT (**p<0.05). (B) Representative western blot of samples following activity assay experiment depicting immunoprecipitated flag-nmMLCK and phosphorylated-MLC. N=3 independent experiments. Standard error bars are shown. MLC, myosin light chain.

Figure 6. VE-cadherin distribution in nmMLCK-transfected Lung EC. Representative confocal microscopy images of EC overexpressing wild-type or mutant GFP-tagged nmMLCK. Images were obtained under basal conditions (A and B) and after treatment with thrombin (1U/ml x 10 min) (C and D). Following treatment cells were fixed on glass coverslips, permeabilized and stained for VE-cadherin (red). Nuclei are stained with DAPI (blue). Transfected cells are indicated by GFP staining in the left image of each pair. In the right image the GFP fluorescence has been subtracted out to provide better visualization of VE-cadherin. After thrombin treatment both wild-type and mutant transfected ECs demonstrate nmMLCK localization to stress fibers. Thrombin results in intercellular gap formation in both wild-type and mutant transfected cells (white arrows). Intercellular VE-cadherin staining appears decreased after thrombin suggestive of a thinning of adherens junctions, but there are no obvious differences between wild-type and mutant transfected cells. Magnified views of VE-cadherin staining at points of cell-cell contact are shown as insets on the right side of each panel. Images are representative of multiple independent experiments.

Supplementary Video. Mutations in nmMLCK alter dynamic cytoskeletal and cell membrane structures. Shown are representative live cell movies of EC co-transfected with wild-type or mutant GFP-tagged nmMLCK constructs and DsRed-CTTN. Cells were imaged under basal conditions for 5 minutes then treated with thrombin (1U/ml) for 10 minutes followed by S1P (1μM) for ~20 minutes. The experimental phase and time (min:seconds) is indicated in

the upper right corner of the videos. The cell transfected with mutant nmMLCK demonstrates more dense stress fiber formation under basal conditions compared to the wild-type cell. While both cells contract in response to thrombin, this is more robust in the cell expressing mutant nmMLCK. After S1P the cell expressing wild-type nmMLCK stops contracting and begins forming lamellipodia, while the cell expressing mutant protein continues to contract and lamellipodia formation is both delayed and blunted.

Figure 1

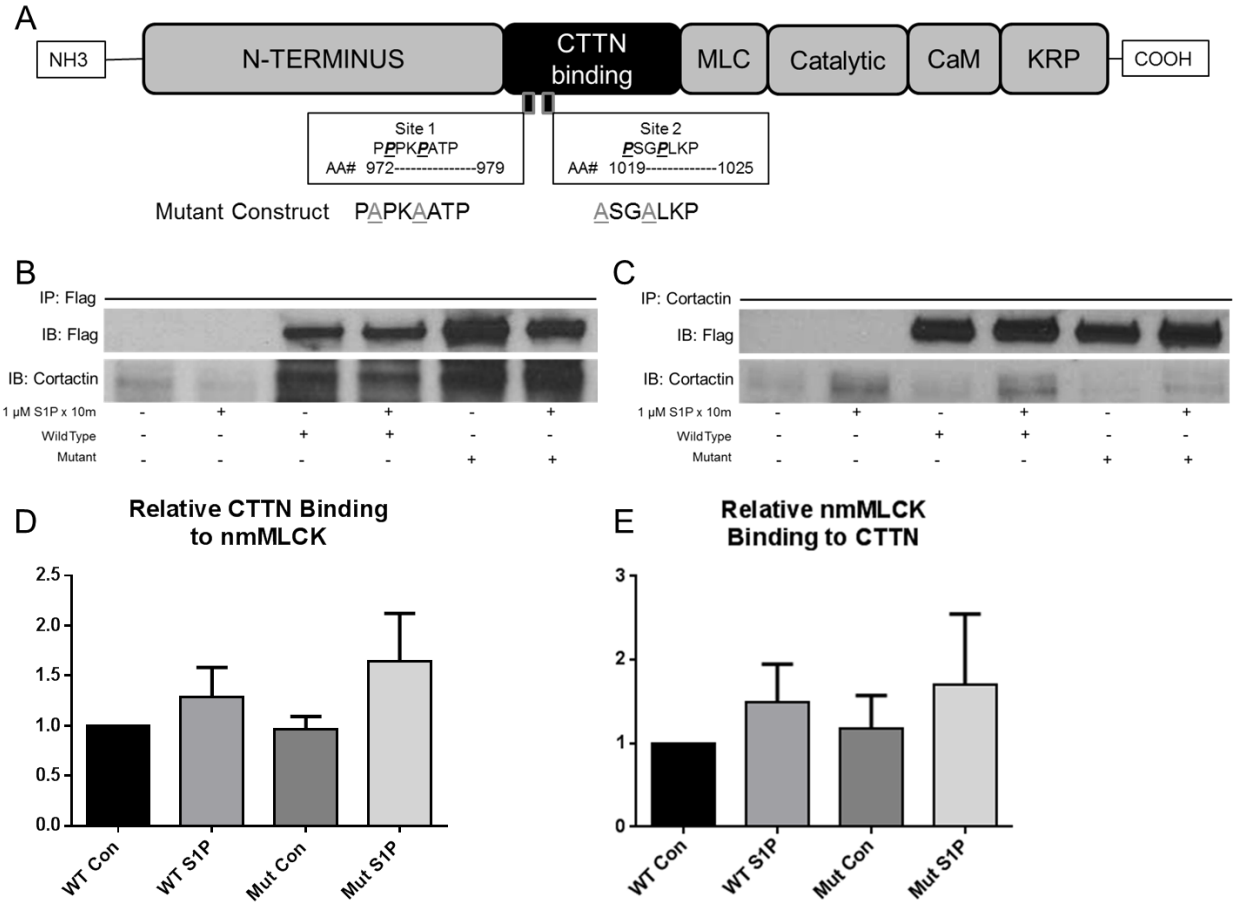
A
NH3
N-TERMINUS
CTTN binding
MLC
Catalytic
CaM
KRP
COOH
Site 1
PPPKPATP
AA# 972----------979
Site 2
PSGPLKP
AA# 1019----------1025
Mutant Construct PAPKAATP ASGALKP
B
IP: Flag
IB: Flag
IB: Cortactin
1 μM S1P x 10m
Wild Type
Mutant
C
IP: Cortactin
IB: Flag
IB: Cortactin
1 μM S1P x 10m
Wild Type
Mutant
D
Relative CTTN Binding to nmMLCK
2.5
2.0
1.5
1.0
0.5
0.0
WT Con
WT S1P
Mut Con
Mut S1P
E
Relative nmMLCK Binding to CTTN
3
2
1
0
WT Con
WT S1P
Mut Con
Mut S1P

Figure 2

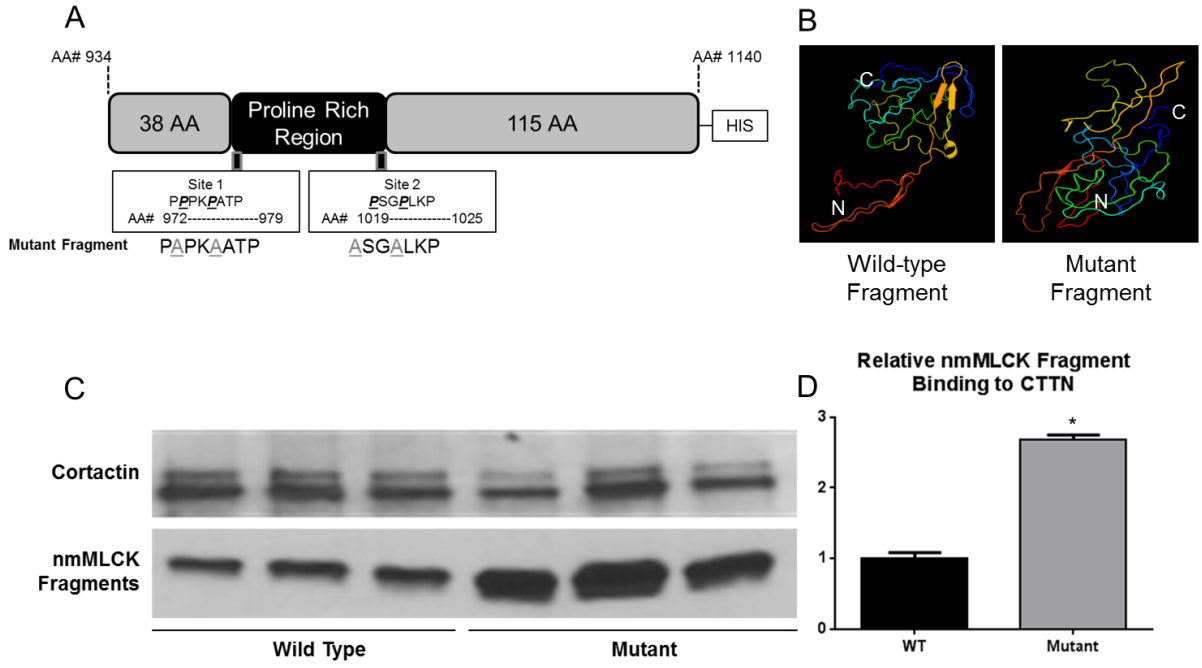
A
AA# 934
AA# 1140
38 AA
Proline Rich Region
115 AA
HIS
Site 1
PPPKPATP
AA# 972----------979
Site 2
PSGPLKP
AA# 1019----------1025
Mutant Fragment
PAPKAATP
ASGALKP
B
C
N
C
N
Wild-type Fragment
Mutant Fragment
C
Cortactin
nmMLCK Fragments
Wild Type
Mutant
D
Relative nmMLCK Fragment Binding to CTTN
3
2
1
0
*
WT
Mutant

Figure 3

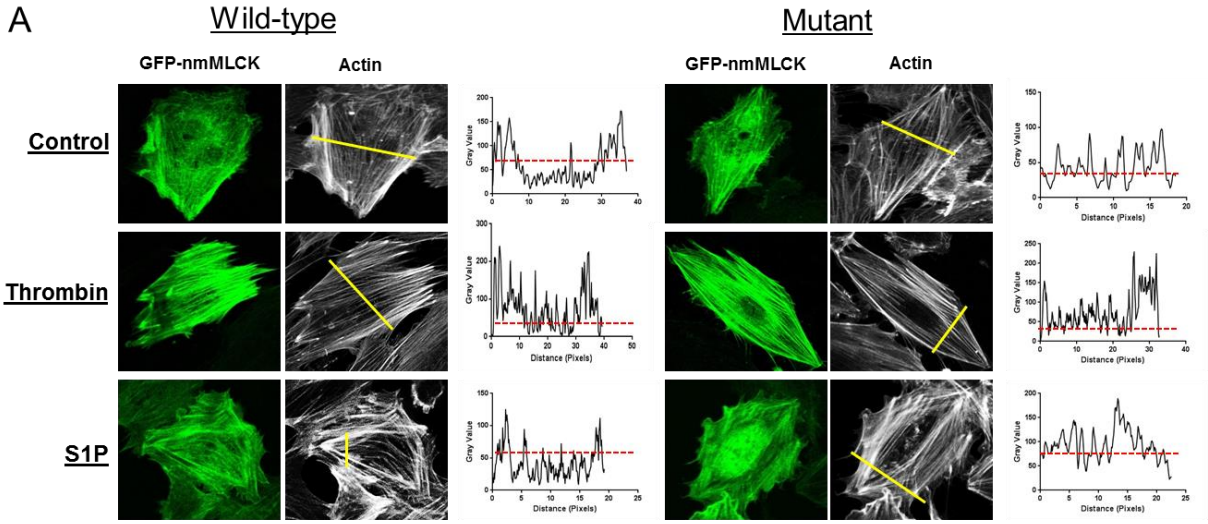
A
Wild-type
Mutant
GFP-nmMLCK
Actin
GFP-nmMLCK
Actin
Control
Thrombin
S1P
Gray Value
Distance (Pixels)

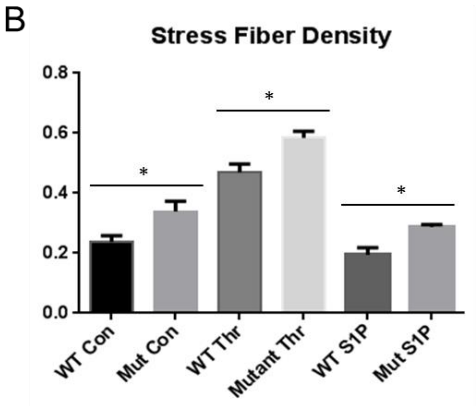
B
Stress Fiber Density
0.8
0.6
0.4
0.2
0.0
*
*
*
WT Con
Mut Con
WT Thr
Mutant Thr
WT S1P
Mut S1P

Figure 4

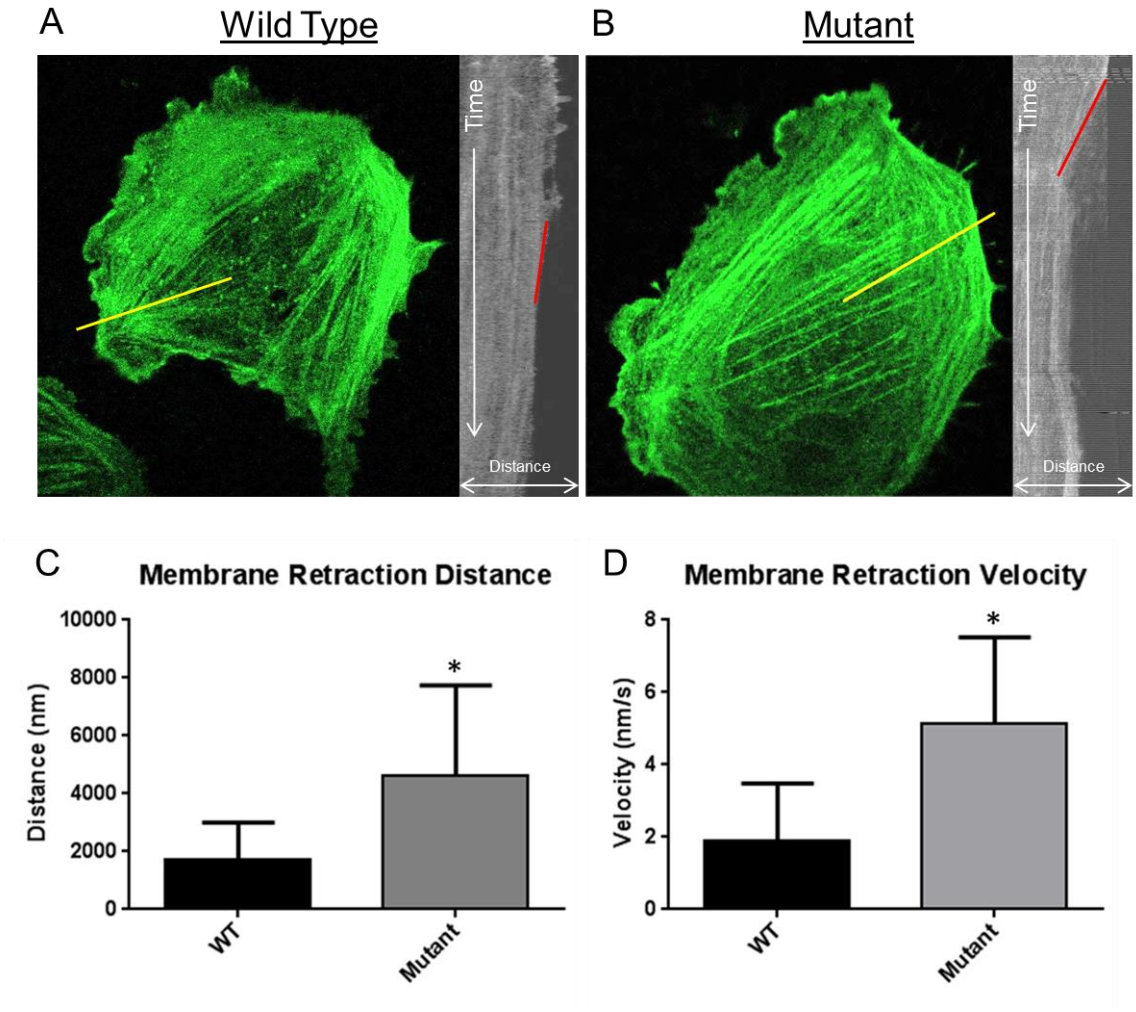
A
Wild Type
B
Mutant
Time
Distance
Time
Distance
C
Membrane Retraction Distance
Distance (nm)
10000
8000
6000
4000
2000
0
*
WT
Mutant
D
Membrane Retraction Velocity
Velocity (nm/s)
8
6
4
2
0
*
WT
Mutant

Figure 5

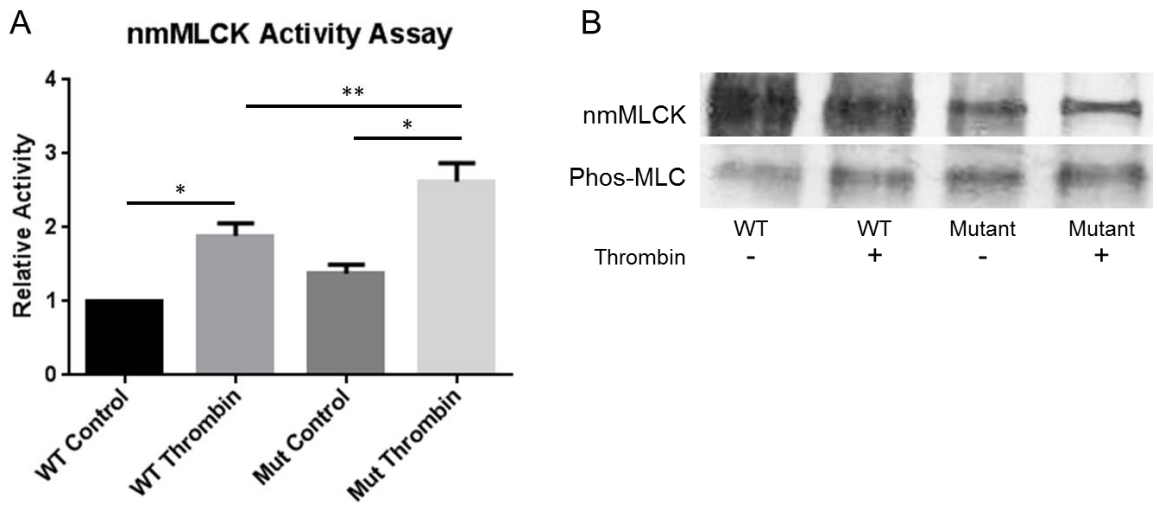

Figure 6